Title

Differential Dorso-ventral Distributions of Kv4.2 and HCN Proteins Confer Distinct Integrative Properties to Hippocampal CA1 Pyramidal Cell Distal Dendrites*

Journal

Journal of Biological Chemistry, 287(21)

ISSN

0021-9258

Authors

Marcelin, Béatrice
Lugo, Joaquin N
Brewster, Amy L
et al.

Publication Date

2012-05-01

DOI

10.1074/jbc.c112.367110

THE JOURNAL OF BIOLOGICAL CHEMISTRY VOL. 287, NO. 21, pp. 17656–17661, May 18, 2012

Differential Dorso-ventral Distributions of Kv4.2 and HCN Proteins Confer Distinct Integrative Properties to Hippocampal CA1 Pyramidal Cell Distal Dendrites*[S]

Received for publication, March 28, 2012 Published, JBC Papers in Press, April 16, 2012, DOI 10.1074/jbc.C112.367110

Béatrice Marcelin[‡§1], Joaquin N. Lugo[¶], Amy L. Brewster[¶2], Zhiqiang Liu[‖], Alan S. Lewis[‖], Shawn McClelland[**], Dane M. Chetkovich[‖‡‡], Tallie Z. Baram[**], Anne E. Anderson[¶§§], Albert Becker[¶¶], Monique Esclapez[‡§], and Christophe Bernard[‡§3]

From the [‡]INSERM, U1106, F-13385 Marseille, France, [§]Aix Marseille Université, F-13385 Marseille, France, the [¶]Cain Foundation Laboratories, Section of Neurology, Department of Pediatrics and the [§§]Department of Neurology and Department of Neuroscience, Baylor College of Medicine, Houston, Texas 77030, the [‖]Davee Department of Neurology and Clinical Neurosciences and the [‡‡]Department of Physiology, Feinberg School of Medicine, Northwestern University, Chicago, Illinois 60611, the [**]Departments of Anatomy/Neurobiology and Pediatrics, University of California, Irvine, California 92697-4475, and the [¶¶]Department of Neuropathology, University of Bonn Medical Center, Sigmund Freud Strasse 25, 53105 Bonn, Germany

Background: Information is differentially processed in the dorsal *versus* ventral hippocampus.
Results: Expression levels of Kv4.2 and HCN1 varied and conferred distinct integrative properties to CA1 pyramidal cell dendrites in dorsal and ventral hippocampus.
Conclusion: Molecular and physiological differences provide the basis for the specific properties of dorsal and ventral CA1 pyramidal cells.
Significance: Channel expression and function enable specific processing roles.

The dorsal and ventral regions of the hippocampus perform different functions. Whether the integrative properties of hippocampal cells reflect this heterogeneity is unknown. We focused on dendrites where most synaptic input integration takes place. We report enhanced backpropagation and theta resonance and decreased summation of synaptic inputs in ventral *versus* dorsal CA1 pyramidal cell distal dendrites. Transcriptional Kv4.2 down-regulation and post-transcriptional hyperpolarization-activated cyclic AMP-gated channel (HCN1/2) up-regulation may underlie these differences, respectively. Our results reveal differential dendritic integrative properties along the dorso-ventral axis, reflecting diverse computational needs.

The dorsal and ventral hippocampal regions are involved in cognitive functions and emotional behavior, respectively (1, 2). This functional segregation has a structural correlate at the gene and connectivity levels (3–6), raising the possibility that neurons in both regions perform different types of computation. The concept of dorso-ventral differences is well established for entorhinal cortex stellate cells, which encode grids of increasing size along the dorso-ventral axis (7). Interestingly, the resonance (or band pass filtering) properties in the soma of these cells also change along this axis, together with the properties of the hyperpolarization-activated I_h current (8–12). Similar principles have been described in CA1 pyramidal cells during development, but whether they persist in adult animals is not known development (13). The size of the place fields coded by CA1 pyramidal cells increases along the dorso-ventral axis (14, 15). Whether this correlates with different integrative properties along this axis remains to be assessed. Because most synaptic integration occurs in dendrites and because dendrites display a heterogeneous distribution of channels as compared with the soma (16), we analyzed the integrative properties of distal dendrites. We focused on three key readouts of dendritic integrative properties: backpropagation of action potentials, resonance, and summation of synaptic inputs (17–20).

When an action potential is generated in the initial segment, it backpropagates to the soma and then to the dendrites. The amplitude of the backpropagating action potential (b-AP)[4] decreases with the distance from the soma because of the activation of the fast transient K^+ current I_A, the density of which increases with the distance from the soma (17). Backpropagating spikes not only inform the dendrites that a spike has been emitted, but also may serve as a trigger for long-term potentiation (16). The main constituent of I_A is the Kv4.2 subunit, which displays remarkable plasticity features in physiological and pathological conditions (21). Modifications in Kv4.2 levels lead

* This work was supported by Institut de la Santé et de la Recherche Médicale, Agence Nationale de la Recherche ANTARES, and MINOS (to C. B.) Deutsche Forschungsgemeinschaft-KForG "Innate Immunity" TP2 (to A. B.), Bundesministerium für Bildung, Wissenschaft, Forschung und Technologie (NGFNplus; to A. B.), European Union EPICURE (to A. B. and C. B.), National Institutes of Health National Research Service Award postdoctoral fellowship (NS056664) (to J. N. L.), National Institutes of Health Grants T32 NS45540 (to S. M.) and T32 NS43124 (to A. L. B.), and National Institutes of Health Grants NS049427 and NS039943 (to A. E. A.) and NS35439 (to T. Z. B.).
[S] This article contains supplemental methods and Figs. 1–5.
[1] Recipient of a Conventions Industrielles de Formation par la REcherche fellowship.
[2] Recipient of an Epilepsy Foundation postdoctoral fellowship.
[3] To whom correspondence should be addressed. E-mail: christophe.bernard@univmed.fr.

[4] The abbreviations used are: b-AP, backpropagating action potential; HCN, hyperpolarization-activated cyclic AMP-gated channel; MΩ, megaohms; EPSP, excitatory postsynaptic potentials; Amp, amplitude.

to changes in dendritic excitability and information processing (21).

Resonance is a property enabling pyramidal and stellate cells to favor inputs in the theta (4–12 Hz) frequency range (19, 20, 22–24), a rhythm involved in numerous cognitive functions (1). Resonance is particularly strong in CA1 pyramidal cell distal dendrites, where it mostly depends upon the activation of the nonspecific cationic hyperpolarization-activated current I_h (19, 20). As for I_A, the density of I_h increases with the distance from the soma (18). It is mainly encoded by the HCN1 and HCN2 subunits, the expression of which also displays remarkable plasticity features in physiological and pathological conditions (21, 25, 26). Modifications in I_h lead to changes in resonance properties and the summation of synaptic inputs (19, 20, 26). Because I_A and I_h appear to be key regulators of dendritic integrative properties, we focused on these two channels and their associated proteins, Kv4.2, HCN1, and HCN2.

EXPERIMENTAL PROCEDURES

Experiments were performed according to local INSERM guidelines.

In Vitro Electrophysiology—Hippocampal 350-μm-thick dorsal (coronal) or ventral (sagittal with a 45° angle) slices were prepared from male adult Wistar Han rats, as described (13). Slices were then transferred to a holding chamber at room temperature in normal artificial cerebrospinal fluid. Artificial cerebrospinal fluid contained (in mM) 126 NaCl, 3.5 KCl, 2 $CaCl_2$, 1.3 $MgCl_2$, 1.2 NaH_2PO_4, 26 $NaHCO_3$, and 10 D-glucose and was continuously aerated with 95% O_2 and 5% CO_2. 2,3-Dihydroxy-6-nitro-7-sulfamoyl-benzo[f]quinoxaline-2,3-dione (1 μM), D-2-amino-5-phosphonovalerate (50 μM), and bicuculline (10 μM) were added to the perfusion solution to block AMPA, NMDA, and $GABA_A$ receptors, respectively. The recording temperature was kept at 34 ± 1 °C (ALA Scientific Instruments). For voltage clamp recordings, patch pipettes were filled with (in mM) 120 $KMeSO_4$, 20 KCl, 0.2 EGTA, 2 $MgCl_2$, 10 HEPES, 4 Na_2ATP, 0.3 Tris GTP, 14 phosphocreatine, and 0.4% biocytin, with KOH to adjust to pH 7.3. Voltages were not corrected for the theoretical −14 mV liquid junction potential. For cell-attached recordings, the solution contained (in mM): 125 NaCl, 10 HEPES, 2.0 $CaCl_2$, 1.0 $MgCl_2$, 2.5 KCl, 1.0 tetrodotoxin, and 0.03 ZD7288.

CA1 pyramidal cell dendrites were recorded under visual control. The distance from the soma was measured both under visual control and post hoc following morphological processing as described previously (27). Dendritic recordings were performed at the border between the stratum radiatum and stratum lacunosum moleculare (see Table 1). There was no difference in access resistance and capacitance between dendrites recorded in the dorsal and ventral parts (see Table 1).

Backpropagation Protocol—Antidromic b-APs were evoked with a stimulation electrode placed at the alveus/stratum oriens border. The amplitude of b-APs was measured at −60 mV. We used depolarizing and hyperpolarizing steps from a starting value of −60 mV to obtain curves giving the amplitude of b-APs as a function of the membrane potential. The transition threshold was defined as the membrane potential when a sudden amplification of the amplitude of the b-AP occurs (28).

Properties of I_A—Ten families of currents were obtained from −85 mV to +55 mV to activate transient (I_A) and sustained K^+ current, as described in Refs. 17–20. The current density of I_A was obtained by calculating $(I_{A\text{-peak}} - I_{sustained})/S$, where S is the surface of the dendritic patch.

Properties of I_h—Currents mediated by I_h were recorded in voltage clamp mode by applying hyperpolarizing voltage steps (from −50 to −140 mV). The amplitude of I_h was determined by subtracting the instantaneous current at the beginning of the voltage step from the steady-state current at the end. The activation time constant was obtained using dual exponential fits. The midpoint activation voltage $V_{½}$ was obtained from the tail current.

Resonance Protocol—Discrete current wavelets at varying frequencies were injected in the recorded cell in current-clamp mode (see Ref. 13). Impedance (Z) was calculated as the ratio of the voltage/current Fast Fourier Transforms: Z = FFT(voltage response)/FFT(injected current), for each frequency. The magnitude of the complex-valued impedance $|Z|$ was plotted against frequency to give an impedance-magnitude profile. Two resonance parameters were measured: Fres, the resonance frequency when $|Z|$ is maximum; and Q, the amplification ratio defined as the $|Z|_{Fres}/|Z|_{1\ Hz}$ ratio.

The impedance phase was calculated as $\phi = \tan^{-1}(\mathrm{Im}(Z)/\mathrm{Re}(Z))$, where $\mathrm{Im}(Z)$ and $\mathrm{Re}(Z)$ are the imaginary and real parts of Z, respectively (29), and tan is the tangent function. F_ϕ is defined as the frequency f where $\phi(f) = 0$. For $f < F_\phi$, the response of the membrane appears to occur before the injected current (phase lead). Conversely, for $f > F_\phi$, there is phase lag. The amount of phase lead was characterized by Φ_L, the area of $\phi(f)$ where $\phi(f) > 0$ (29).

Temporal Summation—Artificial excitatory postsynaptic potentials (EPSPs) were evoked by current injections of the form of an α function: $I = I_{max}\, t \exp(-\alpha t)$, with $\alpha = 0.1$. The temporal summation ratio in a train of five artificial EPSPs was computed as EPSP5/EPSP1, where EPSP5 and EPSP1 are the amplitudes of first and fifth artificial EPSPs in the train, respectively.

Morphology—After electrophysiological recordings, slices were fixed overnight at 4 °C in a solution containing 4% paraformaldehyde in 0.1 M phosphate buffer (pH 7.4). Detection of labeled neurons was performed on unsectioned slices as described (27).

Tissue Preparation and Western Blotting—Animals were killed, and *in toto* hippocampi were rapidly dissected and divided into three parts along the septo-temporal axis: dorsal part, intermediate part, and ventral part. Samples were frozen in liquid nitrogen and stored at −80 °C until tissue processing. To determine Kv4.2 expression levels, total homogenate from samples was created using previously described methods (30). Different tissue samples (from different animals) were also processed using crude synaptosomes for Western blotting. This method has previously been shown to produce synaptosome enrichment in brain tissue (31).

Western blotting for total HCN1, HCN2, and TRIP8b in dorsal and ventral hippocampus was performed as described previously, with sample loading differences controlled by normalizing to α-tubulin (32). Quantitative analysis of the density of

immunoreactive bands was performed with the National Institutes of Health ImageJ or Scion Image software.

mRNA Isolation of Hippocampi and Real-time RT-PCR—Samples were prepared and stored at −80 °C as above. mRNA from the dorsal and ventral hippocampus was isolated by the Dynabeads mRNA DIRECT micro kit (Dynal, Oslo) according to the manufacturer's protocol. Kv4.2, HCN1, and HCN2 transcript quantification was performed by real-time RT-PCR (PE Biosystems PRISM 7700, Foster City). Synaptophysin was used as endogenous, neuron-specific reference gene for normalization of Kv4.2 and HCN channel subunit mRNAs.

Chemicals—All chemicals and drugs were obtained from Sigma or Ascent unless specified otherwise.

Statistics—We used nonparametric Mann-Whitney test for samples lower than 6, and Student's *t* test otherwise. Results are expressed as mean ± S.E., with $p < 0.05$ considered significant.

TABLE 1

Data summary of the basic properties of CA1 pyramidal cell dendrites

All recorded dendrites were divided in two groups depending whether they were used to assess backpropagation or resonance (from different animals). *, $p < 0.05$ between dorsal and ventral. pF, picofarads. RMP, Resting Membrane Potential; Rin, input resistance; C, capacitance; RS, series resistance.

Basic properties	Backpropagation (dorsal) ($n = 12$)	Backpropagation (ventral) ($n = 14$)	Resonance (dorsal) ($n = 24$)	Resonance (ventral) ($n = 22$)
Distance (μm)	321 ± 7	310 ± 12	306 ± 5	307 ± 6
RMP (mV)	−62.8 ± 0.4	−60.7 ± 0.5*	−62.1 ± 0.5	−60.5 ± 0.4*
Rin (MΩ)	50 ± 4	35 ± 5*	57 ± 3	43 ± 3*
C (pF)	72 ± 4	76 ± 5	79 ± 4	88 ± 7
RS (MΩ)	27 ± 2	28 ± 2	26 ± 1	26 ± 2

RESULTS

Current clamp recordings were performed in distal CA1 pyramidal cell dendrites at a similar distance from the soma in the ventral and dorsal hippocampus, all close to the border between the stratum radiatum and stratum lacunosum moleculare (Table 1). There were no obvious morphological differences in the dendritic arbor of neurons recorded in the dorsal and ventral hippocampi (not shown, but see supplemental Fig. 2). Distal dendrites from the ventral hippocampus were slightly more depolarized and had a lower input resistance than dendrites from the dorsal hippocampus (Table 1). Stimulation of CA1 pyramidal cell axons evoked antidromic action potentials,

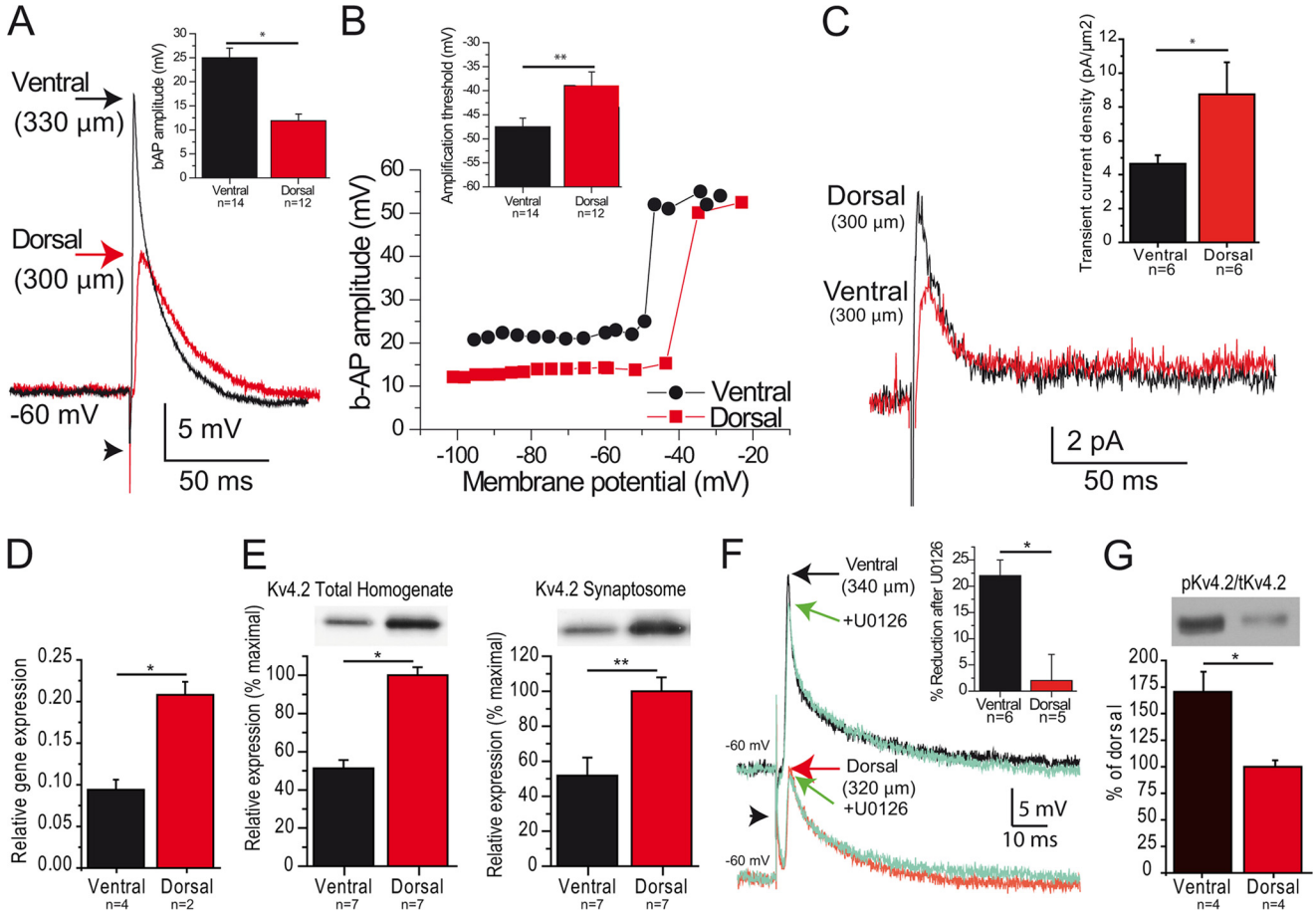

FIGURE 1. **Backpropagation is enhanced in ventral hippocampus.** *A*, example of b-APs recorded in CA1 pyramidal cell distal dendrites from the ventral (*black*) and dorsal (*red*) hippocampus. The *arrowhead* indicates the stimulus artifact. *Inset*, summary of b-AP amplitude in dorsal and ventral hippocampus. *B*, variation of the amplitude of b-APs as a function of membrane potential (same dendrites as in *A*). Note the sharp amplification marking the transition threshold. *Inset*, summary of transition threshold potential in dorsal and ventral hippocampus. *C*, dendritic cell-attached recordings reveal a larger amplitude of the transient A-type current in dorsal *versus* ventral cells (measured at +55 mV), whereas the amplitude of the sustained K^+ current appears similar. *Inset*, summary of current density of A-type current in dorsal and ventral hippocampus. *D* and *E*, Kv4.2 expression is twice larger in the dorsal than in the ventral part of the hippocampus at the mRNA (*D*), total protein (*E*, *left panel*), and synaptosome protein (*E*, *right panel*) levels. *F*, the MEK inhibitor U0126 significantly reduced b-AP amplitude in ventral but not dorsal dendrites. *G*, the ERK-dependent phosphorylation of Kv4.2 was larger in the ventral than in the dorsal hippocampus. *, $p < 0.05$; **, $p < 0.01$.

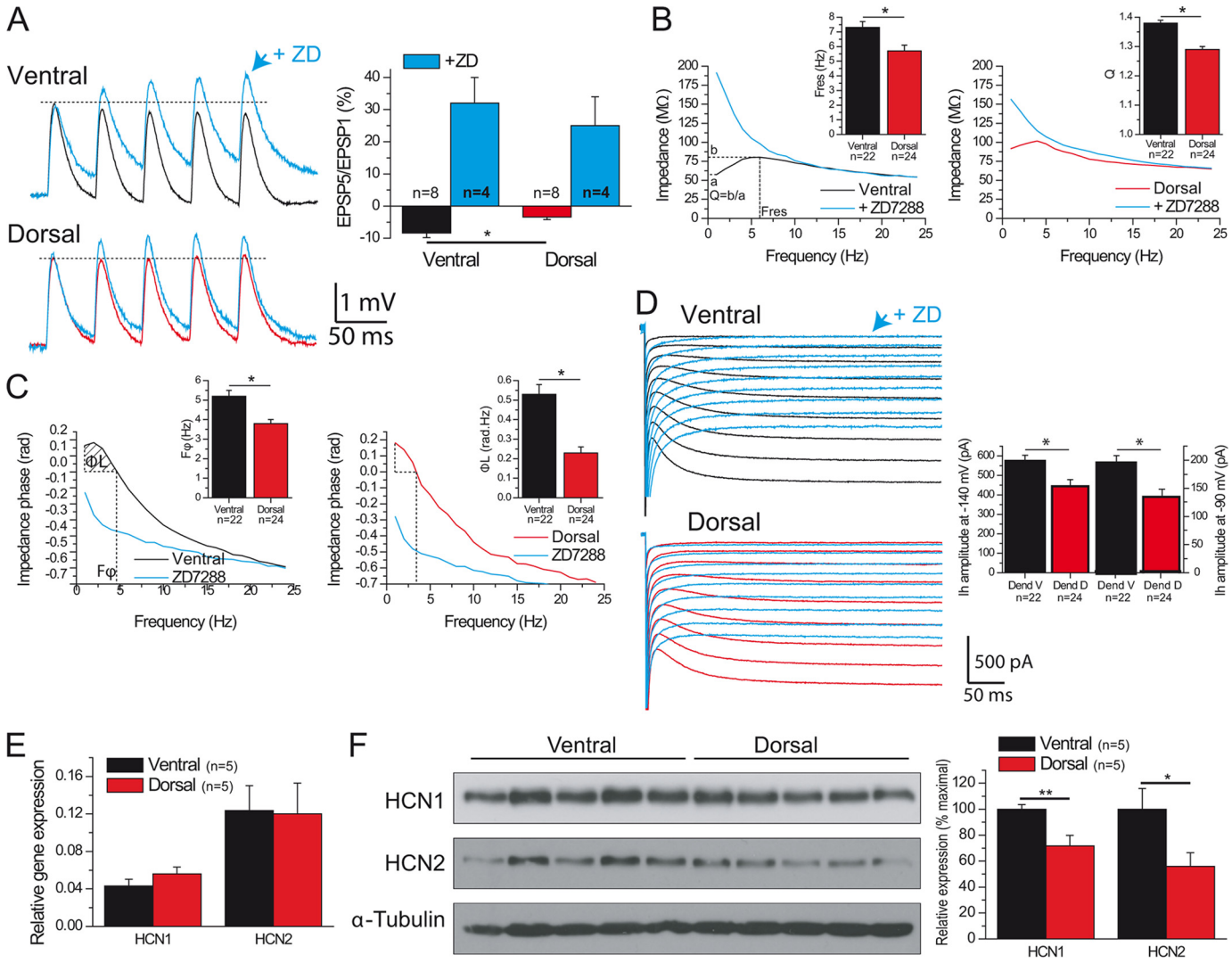

FIGURE 2. **Decreased temporal summation and increased theta resonance and phase lead in ventral hippocampus.** *A*, temporal summation is decreased in ventral *versus* dorsal dendrites. The difference is abolished in the presence of ZD7288 (*ZD*). *B*, *left* and *right panels*, impedance magnitude as a function of the input frequency in a ventral (*left*) or dorsal (*right*) distal dendrite before (*black trace*) and after 10 μM ZD7288 (*red trace*). *Insets*, histograms of resonance parameters. *C*, same as *B* for phase responses. *rad*, radian. *D*, I_h activation curves in ventral and dorsal dendrites, same dendrites as in *B*, showing a larger I_h current in ventral dendrites. I_h activation was blocked by ZD7288. *Inset*, histograms of I_h amplitude measured at −140 mV and −90 mV. *E*, HCN1 and HCN2 mRNA levels are similar in the dorsal and ventral hippocampus. *F*, Western blots demonstrate that HCN1 and HCN2 protein levels are increased in ventral *versus* dorsal hippocampus. *, $p < 0.05$; **, $p < 0.01$.

which backpropagated to dendrites. The amplitude of b-APs was increased by 50% in ventral *versus* dorsal dendrites (Fig. 1*A*, Tables 1 and 2). The transition threshold was depolarized by 10 mV in dorsal *versus* ventral dendrites (Fig. 1*B*, Table 2).

The amplitude of b-APs is inversely related to the availability of A-type K^+ channel, in particular of its main subunit Kv4.2 (17, 33). Cell-attached recordings showed an increased density of I_A in dorsal (8.7 ± 1.9 pA/μm^2, $n = 6$) as compared with ventral (4.7 ± 0.5 pA/μm^2, $n = 6$, $p < 0.05$) distal dendrites (Fig. 1*C*). In keeping with the increase in A-type currents, RT-PCR revealed that Kv4.2 mRNA expression was twice larger in dorsal than ventral hippocampus (Fig. 1*D*). The transcriptional differences translated into similar differences in Kv4.2 protein levels in total homogenates and synaptosomes (Fig. 1*E*). Immunohistochemistry confirmed that the optical density of the Kv4.2 signal quantified per that of the dendritic marker MAP2 was increased in dorsal *versus* ventral hippocampus (supplemental methods, supplemental Fig. 1).

Phosphorylation can affect A-type K^+ channel properties and thus influence the amplitude of b-APs. The extracellular signal-regulated kinase (ERK) can phosphorylate Kv4.2, decrease its activity, and increase backpropagation (33, 34). Blocking ERK through bath application of 10 μM U0126 decreased b-APs in ventral but not in dorsal cells (Fig. 1*F*). This suggests a stronger endogenous ERK phosphorylation of Kv4.2 in ventral cells, which was confirmed at the molecular level (Fig. 1*G*). These results suggest that decreased expression levels of Kv4.2, involving transcriptional regulation, and increased ERK-dependent phosphorylation account, at least in part, for the enhanced backpropagation in ventral CA1 pyramidal cells.

In addition to backpropagation, temporal summation and resonance are critical determinants of dendritic integrative

TABLE 2
Data summary
Amplitude and transition threshold of b-APs. Resonance frequency, amplification ratio, phase responses, and I_h properties (amplitude measured at −140 and −90 mV, half-activation potential, fast and slow time constants). *, $p < 0.05$, **, $p < 0.01$ between dorsal and ventral. rad, radians.

	Dorsal ($n = 12$)	Ventral ($n = 14$)	Dorsal ($n = 12$)	Ventral ($n = 14$)
	Amp = 12 ± 1 mV	Amp = 25 ± 2 mV**	Threshold = −39 ± 3 mV	Threshold = −48 ± 3 mV*
b-AP	Dorsal ($n = 24$)	Ventral ($n = 22$)	Dorsal ($n = 24$)	Ventral ($n = 22$)
Resonance	Fres = 5.7 ± 0.4 Hz	Fres = 7.3 ± 0.4 Hz*	Q = 1.29 ± 0.01	Q = 1.38 ± 0.01*
Phase	F_ϕ = 3.8 ± 0.2 Hz	F_ϕ = 5.2 ± 0.3 Hz*	Φ_L = 0.23 ± 0.03 rad.Hz	Φ_L = 0.53 ± 0.05 rad.Hz*
I_h Amp	−140 mV, 444 ± 34 pA	−140 mV, 566 ± 37 pA*	−90 mV, 134 ± 9 pA	−90 mV, 192 ± 13 pA*
I_h $V_{1/2}$	−101.4 ± 1.2 mV	−101.0 ± 1.4 mV		
I_h τ	Fast: 23 ± 1 ms	Fast: 22 ± 1 ms	Slow: 151 ± 18 ms	Slow: 194 ± 24 ms

properties. Temporal summation was decreased in ventral as compared with dorsal dendrites (Fig. 2*A*; ventral, −8.4 ± 1.4%, $n = 8$; dorsal, −3.4 ± 0.8%, $n = 8$; $p < 0.03$). In keeping with the fact that I_h modulates temporal summation (18), the dorso-ventral difference was abolished in the presence of the I_h antagonist ZD7288 (Fig. 2*A*; ventral, 32 ± 8%, $n = 4$; dorsal, 25 ± 9%, $n = 4$; $p = 0.42$).

CA1 pyramidal cell dendrites efficiently act as band-pass filters in the theta frequency range (4–12 Hz), a property called resonance, which is in part I_h-dependent in the dendrites (19, 20). Resonance and phase lead were stronger in ventral than dorsal dendrites (Table 2; Fig. 2, *B* and *C*, supplemental Figs. 2 and 3). ZD7288 abolished resonance and phase lead (Fig. 2, *B* and *C*; $n = 4$ ventral; $n = 4$ dorsal, supplemental Figs. 2 and 3).

Resonance, phase responses, and temporal summation differences depend, in part, upon I_h properties. The amplitude of I_h was larger in ventral than dorsal dendrites, whereas its kinetics were not different (Table 2; Fig. 2*D*). The percentage of sag, which also depends upon I_h (19), was also larger in ventral than dorsal dendrites (supplemental Fig. 4). In keeping with the stronger contribution of I_h, the resting membrane potential was more depolarized, and the input resistance decreased in ventral *versus* dorsal dendrites (Table 1). Although there was no difference in the mRNA levels of the principal isoforms HCN1 and HCN2 (Fig. 2*E*), protein expression was significantly larger in ventral than dorsal hippocampus (Fig. 2*F*). The synaptosome fraction of HCN1 protein was similarly increased in the ventral hippocampus (supplemental Fig. 5). The optical density of HCN1 signal was increased in ventral *versus* dorsal hippocampus (supplemental Fig. 1).

The auxiliary protein TRIP8b is a key regulator of HCN channels in physiological and pathological conditions (32, 35, 36). However, the expression of TRIP8b was similar in the dorsal and ventral hippocampus. (supplemental Fig. 5). Together, these results suggest that different expression levels of HCN1/2 contribute to the differences in resonance, phase response, and temporal summation in the dorsal and ventral hippocampus.

DISCUSSION

We have shown that Kv4.2, HCN1, and HCN2 expression levels are heterogeneously distributed between the dorsal and ventral hippocampus. This heterogeneity is superimposed upon the gradient of Kv4.2 and HCN along the somato-dendritic axis in CA1 pyramidal cells (17, 18). Functionally, this translates into increased backpropagation, theta resonance, phase lead, and decreased summation in ventral CA1 pyramidal cell dendrites. How these different integrative properties impact information processing, *e.g.* enlargement of place fields (14) or different synaptic plasticity properties (37) from the dorsal to the ventral hippocampus, remains to be addressed. However, our results clearly demonstrate that CA1 pyramidal cells constitute a heterogeneous cell population along the dorso-ventral axis in terms of integrative properties and channel expression in their dendrites.

The mechanisms responsible for the differential expression of Kv4.2 and HCN remain to be determined. In more simple organisms, the expression of certain channels is controlled in a coordinated manner, *i.e.* they appear to co-vary (38). In the present study, Kv4.2 and HCN1 co-vary in opposite directions, and our results suggest that both ion channels are regulated at multiple levels, including transcriptional, translational, and post-translational.

We focused on I_A and I_h because their distribution and function are well documented in the CA1 pyramidal cell dendrites. However, these dendrites express a large array of ionic channels, each relating to specific distribution patterns along the somato-dendritic axis (16). For example, Ca^{2+} channels and the persistent sodium channel also control the integrative properties of CA1 pyramidal cell dendrites (16), including temporal summation and resonance, although not in the range of membrane potentials used here. It is likely that these channels also display dorso-ventral differences.

Surprisingly, the dorso-ventral gradient of resonance and I_h properties of CA1 pyramidal cell dendrites are reversed as compared with those found at earlier stages of development (13). The meaning and mechanisms for such changes remain to be determined. The gradient is also reversed as compared with the soma of layer II stellate cells (10, 12). Although entorhinal cortex stellate cells and CA1 pyramidal cells are not directly connected to each other, these different rules of organization may influence the way the hippocampus and the entorhinal cortex exchange information.

In conclusion, the gene mapping of the hippocampus revealed different regional organizations along the dorso-ventral axis (3, 4, 6). Our results demonstrate that this regional segregation is also true at the protein level, which translates into different functional properties in the dorsal and ventral hippocampus.

Acknowledgment—We thank M. P. Nesa for technical assistance.

REFERENCES

1. Buzsaki, G. (2006) *Rhythms of the Brain*, Oxford University Press Inc., New York
2. Segal, M., Richter-Levin, G., and Maggio, N. (2010) Stress-induced dynamic routing of hippocampal connectivity: a hypothesis. *Hippocampus* **20,** 1332–1338
3. Lein, E. S., Hawrylycz, M. J., Ao, N., Ayres, M., Bensinger, A., Bernard, A., Boe, A. F., Boguski, M. S., Brockway, K. S., *et al*. (2007) Genome-wide atlas of gene expression in the adult mouse brain. *Nature* **445,** 168–176
4. Thompson, C. L., Pathak, S. D., Jeromin, A., Ng, L. L., MacPherson, C. R., Mortrud, M. T., Cusick, A., Riley, Z. L., Sunkin, S. M., Bernard, A., Puchalski, R. B., Gage, F. H., Jones, A. R., Bajic, V. B., Hawrylycz, M. J., and Lein, E. S. (2008) Genomic anatomy of the hippocampus. *Neuron* **60,** 1010–1021
5. van Strien, N. M., Cappaert, N. L., and Witter, M. P. (2009) The anatomy of memory: an interactive overview of the parahippocampal-hippocampal network. *Nat. Rev. Neurosci.* **10,** 272–282
6. Leonardo, E. D., Richardson-Jones, J. W., Sibille, E., Kottman, A., and Hen, R. (2006) Molecular heterogeneity along the dorsal-ventral axis of the murine hippocampal CA1 field: a microarray analysis of gene expression. *Neuroscience* **137,** 177–186
7. Brun, V. H., Solstad, T., Kjelstrup, K. B., Fyhn, M., Witter, M. P., Moser, E. I., and Moser, M. B. (2008) Progressive increase in grid scale from dorsal to ventral medial entorhinal cortex. *Hippocampus* **18,** 1200–1212
8. Giocomo, L. M., and Hasselmo, M. E. (2009) Knock-out of HCN1 subunit flattens dorsal-ventral frequency gradient of medial entorhinal neurons in adult mice. *J. Neurosci.* **29,** 7625–7630
9. Giocomo, L. M., and Hasselmo, M. E. (2008) Time constants of h current in layer ii stellate cells differ along the dorsal to ventral axis of medial entorhinal cortex. *J. Neurosci.* **28,** 9414–9425
10. Giocomo, L. M., Zilli, E. A., Fransén, E., and Hasselmo, M. E. (2007) Temporal frequency of subthreshold oscillations scales with entorhinal grid cell field spacing. *Science* **315,** 1719–1722
11. Boehlen, A., Heinemann, U., and Erchova, I. (2010) The range of intrinsic frequencies represented by medial entorhinal cortex stellate cells extends with age. *J. Neurosci.* **30,** 4585–4589
12. Garden, D. L., Dodson, P. D., O'Donnell, C., White, M. D., and Nolan, M. F. (2008) Tuning of synaptic integration in the medial entorhinal cortex to the organization of grid cell firing fields. *Neuron* **60,** 875–889
13. Marcelin, B., Liu, Z., Chen, Y., Lewis, A. S., Becker, A., McClelland, S., Chetkovich, D. M., Migliore, M., Baram, T. Z., Esclapez, M., and Bernard, C. (2012) Dorsoventral differences in intrinsic properties in developing CA1 pyramidal cells. *J. Neurosci.* **32,** 3736–3747
14. Kjelstrup, K. B., Solstad, T., Brun, V. H., Hafting, T., Leutgeb, S., Witter, M. P., Moser, E. I., and Moser, M. B. (2008) Finite scale of spatial representation in the hippocampus. *Science* **321,** 140–143
15. O'Keefe, J., and Nadel, L. (1978) *The Hippocampus as a Cognitive Map*, Oxford University, Oxford
16. Johnston, D., and Narayanan, R. (2008) Active dendrites: colorful wings of the mysterious butterflies. *Trends Neurosci.* **31,** 309–316
17. Hoffman, D. A., Magee, J. C., Colbert, C. M., and Johnston, D. (1997) K^+ channel regulation of signal propagation in dendrites of hippocampal pyramidal neurons. *Nature* **387,** 869–875
18. Magee, J. C. (1998) Dendritic hyperpolarization-activated currents modify the integrative properties of hippocampal CA1 pyramidal neurons. *J. Neurosci.* **18,** 7613–7624
19. Narayanan, R., and Johnston, D. (2007) Long-term potentiation in rat hippocampal neurons is accompanied by spatially widespread changes in intrinsic oscillatory dynamics and excitability. *Neuron* **56,** 1061–1075
20. Marcelin, B., Chauvière, L., Becker, A., Migliore, M., Esclapez, M., and Bernard, C. (2009) h channel-dependent deficit of theta oscillation resonance and phase shift in temporal lobe epilepsy. *Neurobiol. Dis.* **33,** 436–447
21. Magee, J. C., and Johnston, D. (2005) Plasticity of dendritic function. *Curr. Opin. Neurobiol.* **15,** 334–342
22. Pike, F. G., Goddard, R. S., Suckling, J. M., Ganter, P., Kasthuri, N., and Paulsen, O. (2000) Distinct frequency preferences of different types of rat hippocampal neurons in response to oscillatory input currents. *J. Physiol.* **529,** 205–213
23. Hutcheon, B., and Yarom, Y. (2000) Resonance, oscillation, and the intrinsic frequency preferences of neurons. *Trends Neurosci.* **23,** 216–222
24. Hu, H., Vervaeke, K., and Storm, J. F. (2002) Two forms of electrical resonance at theta frequencies, generated by M-current, h-current, and persistent Na^+ current in rat hippocampal pyramidal cells. *J. Physiol.* **545,** 783–805
25. Noam, Y., Bernard, C., and Baram, T. Z. (2011) Toward an integrated view of HCN channel role in epilepsy. *Curr. Opin. Neurobiol.* **21,** 873–879
26. McClelland, S., Flynn, C., Dubé, C., Richichi, C., Zha, Q., Ghestem, A., Esclapez, M., Bernard, C., and Baram, T. Z. (2011) Neuron-restrictive silencer factor-mediated hyperpolarization-activated cyclic nucleotide gated channelopathy in experimental temporal lobe epilepsy. *Ann. Neurol.* **70,** 454–464
27. Esclapez, M., Hirsch, J. C., Ben-Ari, Y., and Bernard, C. (1999) Newly formed excitatory pathways provide a substrate for hyperexcitability in experimental temporal lobe epilepsy. *J. Comp. Neurol.* **408,** 449–460
28. Bernard, C., and Johnston, D. (2003) Distance-dependent modifiable threshold for action potential backpropagation in hippocampal dendrites. *J. Neurophysiol.* **90,** 1807–1816
29. Narayanan, R., and Johnston, D. (2008) The h channel mediates location dependence and plasticity of intrinsic phase response in rat hippocampal neurons. *J. Neurosci.* **28,** 5846–5860
30. Lugo, J. N., Barnwell, L. F., Ren, Y., Lee, W. L., Johnston, L. D., Kim, R., Hrachovy, R. A., Sweatt, J. D., and Anderson, A. E. (2008) Altered phosphorylation and localization of the A-type channel, Kv4.2, in status epilepticus. *J. Neurochem.* **106,** 1929–1940
31. Lu, H. C., She, W. C., Plas, D. T., Neumann, P. E., Janz, R., and Crair, M. C. (2003) Adenylyl cyclase I regulates AMPA receptor trafficking during mouse cortical "barrel" map development. *Nat. Neurosci.* **6,** 939–947
32. Lewis, A. S., Schwartz, E., Chan, C. S., Noam, Y., Shin, M., Wadman, W. J., Surmeier, D. J., Baram, T. Z., Macdonald, R. L., and Chetkovich, D. M. (2009) Alternatively spliced isoforms of TRIP8b differentially control h channel trafficking and function. *J. Neurosci.* **29,** 6250–6265
33. Yuan, L. L., Adams, J. P., Swank, M., Sweatt, J. D., and Johnston, D. (2002) Protein kinase modulation of dendritic K^+ channels in hippocampus involves a mitogen-activated protein kinase pathway. *J. Neurosci.* **22,** 4860–4868
34. Bernard, C., Anderson, A., Becker, A., Poolos, N. P., Beck, H., and Johnston, D. (2004) Acquired dendritic channelopathy in temporal lobe epilepsy. *Science* **305,** 532–535
35. Santoro, B., Wainger, B. J., and Siegelbaum, S. A. (2004) Regulation of HCN channel surface expression by a novel C-terminal protein-protein interaction. *J. Neurosci.* **24,** 10750–10762
36. Zolles, G., Wenzel, D., Bildl, W., Schulte, U., Hofmann, A., Müller, C. S., Thumfart, J. O., Vlachos, A., Deller, T., Pfeifer, A., Fleischmann, B. K., Roeper, J., Fakler, B., and Klöcker, N. (2009) Association with the auxiliary subunit PEX5R/Trip8b controls responsiveness of HCN channels to cAMP and adrenergic stimulation. *Neuron* **62,** 814–825
37. Maggio, N., and Segal, M. (2007) Unique regulation of long term potentiation in the rat ventral hippocampus. *Hippocampus* **17,** 10–25
38. Schulz, D. J., Goaillard, J. M., and Marder, E. E. (2007) Quantitative expression profiling of identified neurons reveals cell-specific constraints on highly variable levels of gene expression. *Proc. Natl. Acad. Sci. U.S.A.* **104,** 13187–13191